Optics Letters

Lyman-α source for laser cooling antihydrogen

G. Gabrielse,[1,2] B. Glowacz,[3] D. Grzonka,[4] C. D. Hamley,[1] E. A. Hessels,[5] N. Jones,[1] G. Khatri,[1] S. A. Lee,[6] C. Meisenhelder,[1] T. Morrison,[1] E. Nottet,[2] C. Rasor,[6] S. Ronald,[6] T. Skinner,[5] C. H. Storry,[5] E. Tardiff,[1] D. Yost,[6] D. Martinez Zambrano,[2,*] and M. Zielinski[3]

[1]Department of Physics, Harvard University, Cambridge, Massachusetts 02138, USA
[2]Department of Physics and Astronomy, Northwestern University, Evanston, Illinois 60208, USA
[3]Faculty of Physics, Astronomy, and Applied Computer Science, Jagiellonian University, 30-059 Krakow, Poland
[4]Forschungzentrum Juelich GmbH, D-52425 Juelich, Germany
[5]Department of Physics and Astronomy, York University, Toronto, Ontario M3J 1P3, Canada
[6]Department of Physics, Colorado State University, Fort Collins, Colorado 80523, USA
*Corresponding author: daniel.mtzz@cern.ch

Received 1 May 2018; accepted 9 May 2018; posted 21 May 2018 (Doc. ID 328396); published 13 June 2018

We present a Lyman-α laser developed for cooling trapped antihydrogen. The system is based on a pulsed Ti:sapphire laser operating at 729 nm that is frequency doubled using an LBO crystal and then frequency tripled in a Kr/Ar gas cell. After frequency conversion, this system produces up to 5.7 μW of average power at the Lyman-α wavelength. This laser is part of the ATRAP experiment at the antiproton decelerator in CERN.

OCIS codes: (020.3320) Laser cooling; (190.2620) Harmonic generation and mixing.

https://doi.org/10.1364/OL.43.002905

Experimental investigations of cold, trapped antihydrogen are of great interest since a spectroscopic comparison of hydrogen with antihydrogen would stringently test the CPT theorem [1–3]. In addition, antihydrogen can be used to study the gravitational acceleration of antimatter [4–6]. Experiments on antihydrogen have advanced significantly in the last few decades—nested Penning traps [7] are now routinely used to produce [8–10] and trap antihydrogen atoms [11,12], the 1S-2S and hyperfine transitions have been observed [13–15], and an initial test of the gravitational acceleration of antihydrogen has been performed [16]. However, there is still a wide discrepancy between the experimental precision obtained in antihydrogen compared with normal hydrogen, and the ultimate potential of experimental studies of cold trapped antihydrogen remains largely untapped.

The relatively low spectroscopic precision currently obtained in antihydrogen experiments is due in large part to the small number of anti-atoms available per trial (∼10) [12,13,17]. While there is a great effort to increase this number, it is difficult to imagine that it would ever approach the $\sim 10^{15}$ atoms/s available in hydrogen spectroscopy. However, the measurement uncertainty can also be reduced by cooling the antihydrogen, since this will simultaneously increase the precision and decrease leading systematic effects [18,19]. For antimatter gravity studies, higher precision requires the average kinetic energy of the atoms to be less than the change in gravitational potential over a magnetic trap [4,5].

While magnetically trapped hydrogen has previously been cooled through evaporation [20], such methods are not realizable in antihydrogen. With so few atoms, collisions are rare and thermalization rates are prohibitively slow. Instead, there is considerable interest in laser cooling antihydrogen using the 1S-2P transition with Lyman-α (Ly-α) radiation at 121.6 nm [4,21,22–25]. The challenge is that Ly-α lasers are notoriously difficult to build and produce relatively low power. The only demonstration of hydrogen laser cooling reduced the temperature from ≈80 to ≈11 mK over 15 min [26]. This was accomplished with a Ly-α source that produced 160 nW of average power with only 2 nW actually delivered to the atoms. While long by typical standards, hour-scale cooling times are reasonable for antihydrogen studies because the high vacuum within the cryogenic apparatus leads to very long trap lifetimes (>1000 s) [12,17].

In [26], hydrogen was laser cooled by directing radiation along only one axis of the trap, and elastic collisions between the hydrogen atoms were relied on to maintain thermal equilibrium. This mechanism is not present in the antihydrogen trap due to a very slow rate of collisions. While some mixing between the trap degrees of freedom can be expected, depending on the specific configuration of the magnetic trap [23], laser cooling antihydrogen could benefit by directing the cooling beam along both radial and axial trap axes. This, along with the relatively large trap volume when the antihydrogen is first formed, highlights the need for additional Ly-α power in antihydrogen studies.

In addition to the average power requirements, the linewidth of the Ly-α radiation should lie below the 1S-2P natural linewidth of 100 MHz in order to approach the Doppler cooling limit (2.4 mK). An additional advantage of a narrow linewidth is the decreased probability of trap loss due to excitation to untrapped magnetic sublevels [27]. A continuous-wave (cw)

Ly-α source would be ideal for cooling, as it would have the narrowest spectrum and the highest cooling rate as saturation intensities are approached [27–29]. However, due to the nonlinear frequency conversions necessary to produce Ly-α radiation, pulsed sources are still able to produce significantly more average power than cw sources. While the highest reported cw Ly-α power is 20 nW [28], pulsed sources using frequency tripling in a Kr/Ar gas mixture typically produce ∼100 nW [25,26,30]. Four-wave mixing schemes using pulsed lasers and multiple wavelengths usually exhibit higher efficiency at the expense of greater complexity [24]. As a recent example, Saito *et al.* demonstrated a pulsed Ly-α source using four-wave mixing in a Kr/Ar cell which produces 100 μW-level average power, although the linewidth of this source appears to be too broad for laser cooling (≈230 GHz) [31].

In this Letter, we present a pulsed Ly-α radiation source, developed for the ATRAP collaboration at CERN, which is suitable for cooling antihydrogen. The source is based on a narrow-linewidth pulsed Ti:sapphire laser system operating at 729 nm, whose frequency is referenced to an optical frequency comb. The 729 nm source is frequency doubled in an LBO nonlinear crystal and then tripled in a Kr/Ar gas cell to produce Ly-α radiation. We chose a solid state fundamental laser and a sextupling process over more complex four-wave mixing schemes to make the system as robust as possible. We generate up to 5.7 μW of average power which is more than 10 times greater than previous demonstrations based on a solid state fundamental laser and a straightforward sextupling process [25].

As shown in Fig. 1, the fundamental laser is composed of a pulsed Ti:sapphire oscillator followed by a multipass amplifier. The oscillator cavity is formed with an output coupler ($R = 80\%$), a concave high reflector (radius-of-curvature = 3 m), and a dispersive prism that provides rough wavelength selectivity. This design aims to produce a large beam radius of 500 μm throughout the cavity which minimizes potential damage to the cavity optics [32]. The Brewster-cut Ti:sapphire crystal is 2 cm long and is doped to absorb 94% of the pump light. The crystal is pumped by 532 nm pulses at a repetition rate of 30 Hz (using a Spectra-Physics Quanta-Ray Pro-290). The pump beam passes through a telescope that relay-images the beam to the crystal and reduces the mode to roughly match the width of the intracavity 729 nm laser mode. While the laser pulses from the pump beam have a 10 ns duration, the pulses from the laser oscillator have a 60 ns duration due to the cavity dynamics and 3.2 μs lifetime of the Ti:sapphire gain medium. With a pump energy of 25 mJ, the oscillator produces 8 mJ pulses at 729 nm.

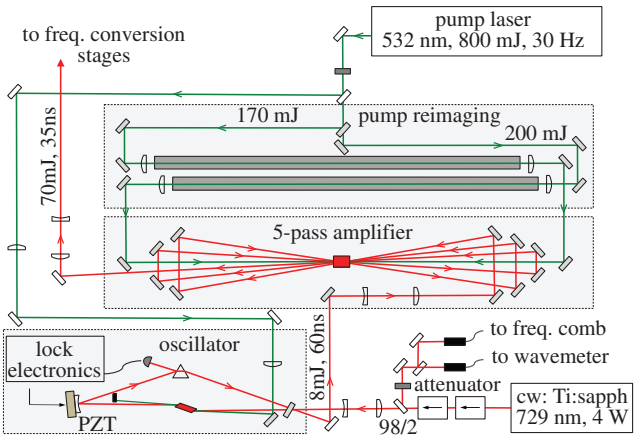

Fig. 1. Fundamental laser: a cw Ti:sapphire laser is used to injection lock a pulsed oscillator at 729 nm (6 times the Ly-α wavelength). The cw laser is locked to a frequency comb, and the comb mode number is determined with a wavemeter. The pulsed oscillator produces 8 mJ pulses with a 60 ns pulse duration and a repetition rate of 30 Hz. This pulse train is then amplified up to 70 mJ in a multipass amplifier before being sent to the frequency conversion stages.

To provide fine frequency control, the oscillator is injection locked with 100 mW of power from a cw Ti:sapphire laser (M Squared: SolsTiS), which is phase locked to an optical frequency comb (Menlo Systems). The curved high reflector is mounted on a piezoelectric transducer (PZT) that is dithered at 200 kHz. A small amount of the intracavity power reflects from the prism and is detected with a photodiode. This signal is demodulated to produce an error signal which is fed back to the PZT through a loop filter to keep the cavity on resonance. Since the peak power is about six orders of magnitude larger than the average power, it would be desirable to block the photodiode for the duration of the pulse (with a Pockel's cell, for example). However, we found that by attenuating the power on the photodiode to the minimum lockable level and applying a low-pass filter to the detector at around 300 kHz, the cavity lock can be maintained during the pulse. A long-throw stack PZT on a translation stage is used to compensate for large slow excursions of the oscillator cavity length. When the injection lock is inactive, the oscillator will lase in both the forward and reverse directions. Therefore, we protect the cw Ti:sapphire seed laser with two optical isolators (>74 dB isolation) and a 98/2 beam splitter to ensure that only a very small fraction of the pulse generated in the reverse direction returns to the cw laser.

The output beam from the laser oscillator is expanded to 5 mm in diameter and sent to a five-pass Ti:sapphire amplifier. The amplifier crystal is 15 mm long and doped to absorb 92% of the incident pump energy. The amplifier is pumped with up to 370 mJ of 532 nm pump power. In order to maintain a good beam quality and to prevent damage to the crystal, the pump beams are relay-imaged to the crystal through vacuum using $f = 1.5$ m and $f = 1$ m lenses. This lens combination also served to reduce the size of the pump beam to 6 mm to roughly match the size of the transverse profile of the 729 nm beam being amplified. The output of the multipass amplifier achieves 70 mJ pulses at a repetition rate of 30 Hz. Although additional 532 nm pump energy is available, the maximum output pulse energy of the amplifier is limited to avoid optical damage to the Ti:sapphire crystal and pump relay-imaging optics.

The frequency conversion and Ly-α detection setup are shown in Fig. 2. The output from the amplifier is frequency doubled in an LBO crystal. The beam size is reduced to ≈2 mm diameter prior to the doubling to optimize the conversion efficiency, while remaining safely below the damage threshold of the crystal. The crystal is 2 cm long and antireflection coated for both the fundamental and second harmonic (729 and 365 nm, respectively). At the highest fundamental pulse energy of 70 mJ, we observe a 30% conversion efficiency which corresponds to a 365 nm pulse energy ($E_{365\,\mathrm{nm}}$) of 21 mJ.

The 365 nm laser pulses are then frequency tripled in a gas cell to generate Ly-α radiation. Prior to conversion, the UV

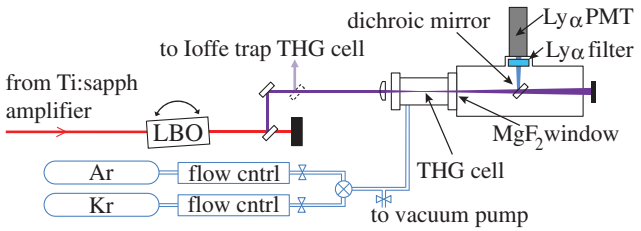

Fig. 2. Frequency conversion and detection setup. The 729 nm pulsed laser is doubled in a non-critically phase-matched LBO crystal (2 cm length) producing 365 nm radiation with 21 mJ of pulse energy and a 30 Hz repetition rate. The UV power is then tripled in a Kr/Ar cell to produce Ly-α radiation which is separated from the 365 nm radiation and sent to a solar blind PMT.

radiation has a transverse beam diameter of ≈1.5 mm, and it is focused near the center of the 20 cm Kr/Ar gas cell using a $f =$ 10 cm lens. The third-order nonlinear susceptibility of Kr is much larger than Ar; the function of the Ar is to compensate for the negative dispersion of the Kr to achieve phase matching [33–35]. In order to ensure that the gases are well mixed, we fill the cell through a static gas mixer using two calibrated mass flow controllers. To maintain gas purity, the cell is constructed out of high vacuum stainless steel components and evacuated with a turbomolecular pump system prior to being filled. The confocal parameter is $b \approx 4$ mm, while the gas cell length is 20 cm which indicates operation in the tight focus regime [36].

The generated Ly-α radiation passes through a MgF_2 window used to seal the gas cell and is detected with a solar blind photomultiplier tube (PMT) with a ≈5% quantum efficiency for Ly-α and a much lower ($<10^{-3}$) quantum efficiency at 365 nm. However, the conversion from 365 nm to Ly-α is only 10^{-6}–10^{-5} efficient, and we found that the 365 nm signal is significant if the full power is incident on the detector. Therefore, we use a custom optic with antireflection coatings for s-polarized 365 nm radiation on both surfaces. The SiO_2 top layer reflects 17% of s-polarized Ly-α so that this optic operates as a dichroic mirror. Since some of the 365 nm radiation will be reflected from this window (≈0.25%), 1–2 Ly-α filters (Acton Optics FN122-XN-1D) are used to further attenuate the 365 nm radiation. A Ly-α discharge lamp with a NIST traceable spectral irradiance is used in place of the gas cell to calibrate the efficiency of the detector and the transmission of the Ly-α filters.

Figure 3 shows the Ly-α yield as a function of Kr and Ar gas pressures within the tripling cell. For low incident energy ($E_{365\,\mathrm{nm}} = 4$ mJ) and a phase-matched Kr/Ar gas mixture, the Ly-α pulse energy ($E_{121\,\mathrm{nm}}$) is roughly proportional to P_{tot}^2, where P_{tot} is the total gas pressure in the cell [36]. However, when $E_{365\,\mathrm{nm}}$ is increased to 20 mJ, the Ly-α energy saturates at around 1.5 bar due to dielectric breakdown. The ideal mixture for phase matching depends on the pulse energy. The Ar gas seems to partially compensate for the negative dispersion introduced with small plasma density, which is absent at low pulse energy. The ideal Ar/Kr mixing ratio turns out to be between 2.05 to 2.3 (depending on the pulse energy), which is in reasonable agreement with previous measurements [33–35].

Figure 4 shows the output Ly-α energy as a function of incident 365 nm energy for $P_{\mathrm{Ar}}/P_{\mathrm{Kr}} = 2.3$ and $P_{\mathrm{tot}} = 1.5$ bar. For low 365 nm pulse energy, $E_{121\,\mathrm{nm}} \propto E_{365\,\mathrm{nm}}^3$, as expected.

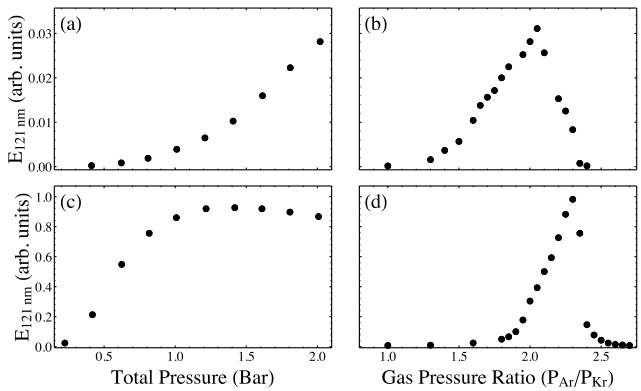

Fig. 3. Optimization of tripling cell partial pressures. (a) $P_{\mathrm{Ar}}/P_{\mathrm{Kr}} = 2.05$, and $E_{365\,\mathrm{nm}} = 4$ mJ. (b) $P_{\mathrm{tot}} = 1.5$ bar, and $E_{365\,\mathrm{nm}} = 4$ mJ. The lower two plots are for increased incident pulse energy. (c) $P_{\mathrm{Ar}}/P_{\mathrm{Kr}} = 2.05$, and $E_{365\,\mathrm{nm}} = 20$ mJ. (d) $P_{\mathrm{tot}} = 1.5$ bar, and $E_{365\,\mathrm{nm}} = 20$ mJ.

At higher pulse energies the output deviates from the cubic trend and saturates due to the ionization of the gas which alters the phase matching. At $E_{365\,\mathrm{nm}} \approx 10$ mJ, the Ly-α yield is slightly higher than the cubic trend since $P_{\mathrm{Ar}}/P_{\mathrm{Kr}}$ was optimized for our highest pulse energy. We obtain a maximum Ly-α pulse energy of $E_{121\,\mathrm{nm}} = 190(40)$ nJ, where the uncertainty follows from our confidence in the detector calibration. Given our 30 Hz repetition rate, this corresponds to 5.7 μW of average optical power. This power is stable for an observed period of more than 2 h.

In converting the pulse train from 729 nm to Ly-α, the individual pulse duration is reduced, since the peak of the pulse is converted more efficiently than the leading and trailing edges.

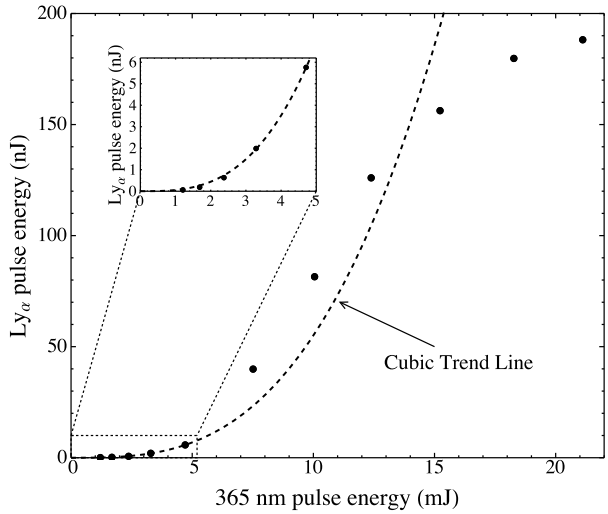

Fig. 4. Ly-α pulse energy ($E_{121\,\mathrm{nm}}$) as a function of incident 365 nm energy ($E_{365\,\mathrm{nm}}$) in a phase-matched mixture of Kr and Ar ($P_{\mathrm{Ar}}/P_{\mathrm{Kr}} = 2.3$ and $P_{\mathrm{tot}} = 1.5$ bar). The dashed line is a cubic fit of the first five data points. As $E_{365\,\mathrm{nm}}$ increases, $E_{121\,\mathrm{nm}}$ saturates to ≈200 nJ. At $E_{365\,\mathrm{nm}} \approx 10$ mJ, the Ly-α yield is slightly higher than that of the cubic trend, since the phase matching is improved for small plasma densities. The measured Ly-α yield was calibrated with a Ly-α lamp. This calibration agreed with the quoted quantum efficiency of the detector to within 20%.

We measured a 365 nm pulse duration of ≈32 ns and a Ly-α pulse duration of ≈16 ns. For a flat phase, the Fourier transform of the measured temporal profile gives a linewidth of ≈25 MHz that is well suited for laser cooling antihydrogen because the 1S-2P transition width is 100 MHz. In practice, there is a frequency chirp generated in the Ti:sapphire crystals due to the fast index of refraction changes when the crystals are pumped [37]. The chirp is measured after the five-pass-amplifier by mixing the pulse train with a frequency-shifted copy of the cw seed beam. The frequency is shifted by 350 MHz using an acousto-optic modulator before mixing. We measure a chirp of 2.5 MHz/(10 ns). This chirp can be corrected below the megahertz level, as recently demonstrated in [38], although not necessary for laser cooling antihydrogen.

The ATRAP lasers and trap are separated by 8 m, and Ly-α must travel in vacuum. The best mirrors at this wavelength are only about 80% reflective, and MgF_2 transmission is between 50 and 60% under ideal conditions. Therefore, we have mounted the tripling gas cells directly on the ATRAP apparatus to reduce the vacuum path length and the number of steering optics and windows.

In conclusion, we have demonstrated a narrowband Ly-α laser with 5.7 μW of average power, which is well suited for laser cooling antihydrogen. In the previous demonstration of hydrogen laser cooling, the system was only able to deliver ≈2 nW of the generated radiation to the atoms [26]. With the increase in Ly-α power reported in this Letter, and by minimizing the Ly-α optics and path length to the trap, we should be able to drastically improve our system in this regard and deliver about 200 nW of the generated radiation to the antihydrogen trap volume. With single-axis cooling, we have modeled that this power level could cool antihydrogen trapped within the ATRAP octopole magnetic trap from 170 to 17 mK in hour timescales [39].

Funding. National Science Foundation (NSF); Air Force Office of Scientific Research (AFOSR).

Acknowledgment. We gratefully acknowledge CERN for providing 5 MeV antiprotons, as well as useful conversations with Yong Wang, Jorge Rocca, Masaki Hori, and Anna Soter. G. Gabrielse acknowledges helpful conversations with S. Rolston.

REFERENCES

1. G. Gabrielse, in *Fundamental Symmetries*, P. Bloch, P. Pavlopoulos, and R. Klapisch, eds. (Plenum, 1987), pp. 59–75.
2. G. Gabrielse, in *Advances in Atomic, Molecular, and Optical Physics*, B. Bederson and H. Walther, eds. (Academic, 2001), Vol. **45**, pp. 1–39.
3. M. Hori and J. Walz, Prog. Part. Nucl. Phys. **72**, 206 (2013).
4. G. Gabrielse, Hyperfine Interact. **44**, 349 (1988).
5. J. Walz and T. W. Hänsch, Gen. Relativ. Gravit. **36**, 561 (2004).
6. The AEGIS Collaboration, Nucl. Instrum. Methods Phys. Res. Sect. B **266**, 351 (2008).
7. G. Gabrielse, L. Haarsma, S. Rolston, and W. Kells, Phys. Lett. A **129**, 38 (1988).
8. The ATRAP Collaboration, Phys. Rev. Lett. **89**, 213401 (2002).
9. The ATRAP Collaboration, Phys. Rev. Lett. **89**, 233401 (2002).
10. The ATHENA Collaboration, Nature **419**, 456 (2002).
11. The ALPHA Collaboration, Nature **468**, 673 (2010).
12. The ATRAP Collaboration, Phys. Rev. Lett. **108**, 113002 (2012).
13. The ALPHA Collaboration, Nature **541**, 506 (2017).
14. The ALPHA Collaboration, Nature **548**, 66 (2017).
15. The ALPHA Collaboration, Nature **557**, 71 (2018).
16. The ALPHA Collaboration, and A. E. Charman, Nat. Commun. **4**, 1785 (2013).
17. The ALPHA Collaboration, Nat. Phys. **7**, 558 (2011).
18. O. J. Luiten, H. G. C. Werij, I. D. Setija, M. W. Reynolds, T. W. Hijmans, and J. T. M. Walraven, Phys. Rev. Lett. **70**, 544 (1993).
19. C. L. Cesar, D. G. Fried, T. C. Killian, A. D. Polcyn, J. C. Sandberg, I. A. Yu, T. J. Greytak, D. Kleppner, and J. M. Doyle, Phys. Rev. Lett. **77**, 255 (1996).
20. N. Masuhara, J. M. Doyle, J. C. Sandberg, D. Kleppner, T. J. Greytak, H. F. Hess, and G. P. Kochanski, Phys. Rev. Lett. **61**, 935 (1988).
21. T. W. Hijmans, O. J. Luiten, I. D. Setija, and J. T. M. Walraven, J. Opt. Soc. Am. B **6**, 2235 (1989).
22. D. Kolbe, A. Beczkowiak, T. Diehl, A. Koglbauer, M. Sattler, M. Stappel, R. Steinborn, and J. Walz, Hyperfine Interact. **212**, 213 (2012).
23. P. H. Donnan, M. C. Fujiwara, and F. Robicheaux, J. Phys. B **46**, 025302 (2013).
24. J. M. Michan, M. C. Fujiwara, and T. Momose, Hyperfine Interact. **228**, 77 (2014).
25. J. M. Michan, G. Polovy, K. W. Madison, M. C. Fujiwara, and T. Momose, Hyperfine Interact. **235**, 29 (2015).
26. I. D. Setija, H. G. Werij, O. J. Luiten, M. W. Reynolds, T. W. Hijmans, and J. T. Walraven, Phys. Rev. Lett. **70**, 2257 (1993).
27. K. S. E. Eikema, J. Walz, and T. W. Hänsch, Phys. Rev. Lett. **83**, 3828 (1999).
28. K. S. E. Eikema, J. Walz, and T. W. Hänsch, Phys. Rev. Lett. **86**, 5679 (2001).
29. M. Scheid, D. Kolbe, F. Markert, T. W. Hänsch, and J. Walz, Opt. Express **17**, 11274 (2009).
30. L. Cabaret, C. Delsart, and C. Blondel, Opt. Commun. **61**, 116 (1987).
31. N. Saito, Y. Oishi, K. Miyazaki, K. Okamura, J. Nakamura, O. A. Louchev, M. Iwasaki, and S. Wada, Opt. Express **24**, 7566 (2016).
32. M. Hori and A. Dax, Opt. Lett. **34**, 1273 (2009).
33. H. Langer, H. Puell, and H. Röhr, Opt. Commun. **34**, 137 (1980).
34. R. Mahon and Y. M. Yiu, Opt. Lett. **5**, 279 (1980).
35. R. Hilbig and R. Wallenstein, IEEE J. Quantum Electron. **17**, 1566 (1981).
36. R. W. Boyd, *Nonlinear Optics*, 3rd ed. (Elsevier, 2008).
37. S. Hannemann, E.-J. Duijn, and W. Ubachs, Rev. Sci. Instrum. **78**, 103102 (2007).
38. C. Cheng, J. Hussels, M. Niu, H. L. Bethlem, K. S. E. Eikema, E. J. Salumbides, W. Ubachs, M. Beyer, N. J. Hölsch, J. A. Agner, F. Merkt, L.-G. Tao, S.-M. Hu, and C. Jungen, "Dissociation energy of the hydrogen molecule at 10^{-9} accuracy," arXiv:1804.11143.
39. N. Jones, Department of Physics, Harvard University, Cambridge, Massachusetts 02138 (personal communication, 2018).